Chemical Science

EDGE ARTICLE

View Article Online
View Journal | View Issue

Cite this: *Chem. Sci.*, 2014, **5**, 3104

Influence of Gb_3 glycosphingolipids differing in their fatty acid chain on the phase behaviour of solid supported membranes: chemical syntheses and impact of Shiga toxin binding†

Ole M. Schütte,‡[a] Annika Ries,‡[a] Alexander Orth,[a] Lukas J. Patalag,[ab] Winfried Römer,[cd] Claudia Steinem*[a] and Daniel B. Werz*[b]

The Shiga toxin B subunit (STxB), which is involved in cell membrane attachment and trafficking of Shiga holotoxin, binds specifically to the glycosphingolipid Gb_3. In biological membranes, Gb_3 glycosphingolipids differ in their fatty acid composition and there is strong evidence that the fatty acid alters the binding behaviour of STxB as well as the intracellular routing of the Shiga toxin/Gb_3 complex. To analyse the binding of STxB to different Gb_3s, we chemically synthesized saturated, unsaturated, α-hydroxylated Gb_3s and a combination thereof, all based on a C_{24}-fatty acid chain starting from monosaccharide building blocks, sphingosine and the respective fatty acids. These chemically well-defined Gb_3s were inserted into solid supported phase-separated lipid bilayers composed of DOPC/sphingomyelin/cholesterol as a simple mimetic of the outer leaflet of animal cell membranes. By fluorescence- and atomic force microscopy the phase behaviour of the bilayer as well as the lateral organization of bound STxB were analysed. The fatty acid of Gb_3 significantly alters the ratio between the ordered and disordered phase and induces a third intermediate phase in the presence of unsaturated Gb_3. The lateral organization of STxB on the membranes varies significantly. While STxB attached to membranes with Gb_3s with saturated fatty acids forms protein clusters, it is more homogeneously bound to membranes containing unsaturated Gb_3s. Large interphase lipid redistribution is observed for α-hydroxylated Gb_3 doped membranes. Our results clearly demonstrate that the fatty acid of Gb_3 strongly influences the lateral organization of STxB on the membrane and impacts the overall membrane organization of phase-separated lipid membranes.

Received 5th May 2014
Accepted 13th May 2014

DOI: 10.1039/c4sc01290a

www.rsc.org/chemicalscience

Introduction

Glycosphingolipids are the cellular receptors of a number of viruses and bacterial toxins. For example, simian virus 40 and other polyoma viruses as well as the bacterial AB_5 protein Cholera toxin tightly attach to the plasma membrane *via* the ganglioside G_{M1} resulting in plasma membrane invaginations.[1,2] Shiga toxin, an AB_5 protein produced by *Shigella dysenteriae* and by enterohemorrhagic strains of *Escherichia coli* (EHEC) binds *via* its homopentameric B-subunits (STxB) to the neutral globoside Gb_3.[3,4] This process is the initial step for Shiga toxin to efficiently enter cells. After endocytosis, Shiga toxin leaves the endocytic pathway at the level of early endosomes following the retrograde transport route.[5] Römer *et al.*[6] showed that the pentameric B-subunits, which can bind up to 15 Gb_3 molecules, induce a clathrin- and caveolin-independent tubule formation upon attachment to HeLa-cells and that invaginations were even found in artificial membranes, when STxB binds to giant unilamellar vesicles (GUVs). These results suggest a significant lipid contribution to the earliest steps of toxin uptake into cells and there are several lines of evidence that the cytotoxicity of Shiga toxin is strongly associated with Gb_3 density and binding to cholesterol-containing lipid rafts.[5,7,8] Following this hypothesis, it has been demonstrated that STxB binding leads to an increased lipid order in cellular membranes.[6] Results obtained from artificial membranes on

[a]*Institute of Organic and Biomolecular Chemistry, University of Göttingen, Tammannstr. 2, 37077 Göttingen, Germany. E-mail: csteine@gwdg.de*

[b]*Institute of Organic Chemistry, Technische Universität Braunschweig, Hagenring 30, 38106 Braunschweig, Germany. E-mail: d.werz@tu-braunschweig.de*

[c]*BIOSS – Centre for Biological Signalling Studies, Albert-Ludwigs-University Freiburg, Schänzlestraße 18, 79104 Freiburg, Germany. E-mail: winfried.roemer@bioss.uni-freiburg.de*

[d]*Institute of Biology II, Albert-Ludwigs-University Freiburg, Schänzlestraße 1, 79104 Freiburg, Germany*

† Electronic supplementary information (ESI) available: Experimental details of the synthesis and analytical data of **27–30**; detailed experimental procedures on the preparation and analysis of solid supported bilayers; fatty acid distribution of natural Gb_3 and bovine brain SM; additional fluorescence and AFM images of phase-separated lipid bilayers; calculation of STxB surface coverage and receptor coverage; ternary phase diagram to estimate phase compositions. See DOI: 10.1039/c4sc01290a

‡ These authors contributed equally to this work.

solid substrates as well as from pore-spanning membranes further showed that STxB is capable of reorganizing lipids within these membranes concomitant with protein cluster formation.[9,10] This process can induce a protein induced local compaction of particular lipids in one leaflet leading to an asymmetric reduction in membrane area, which is prerequisite for membrane invaginations.[11]

In all these studies, mixtures of Gb_3 from natural sources have been used, which are composed of Gb_3 molecules with different fatty acid compositions. Even though the Gb_3-concentration is only a few mol% in these membranes, there is strong evidence that the fatty acid composition of Gb_3 significantly influences the process of Shiga toxin binding,[12] membrane organization,[9,13] invagination,[6] and scission.[14] Lingwood and coworkers found that Gb_3s with long fatty acid chains (C_{20}–C_{24}) bind Shiga toxin with higher affinity than those with short fatty acid chains (C_{12}, C_{14}).[15] Also, the α-hydroxylation of the fatty acid of Gb_3 gave rise to a larger binding affinity and larger binding capacity of STxB compared to the non-hydroxylated fatty acid.[13] Besides the observed differences in the STxB binding behaviour, α-hydroxylated fatty acids attached to glycolipids have also been shown to strongly influence local membrane organization owing to their ability to form hydrogen bonds.[16–18] However, as yet there is no systematic study available addressing the impact of the fatty acid composition of Gb_3 on the organization of lipid membranes that partially mimic the composition of the outer leaflet of animal plasma membranes. This arises from the fact that, apart from some reports on semisynthetic approaches to generate Gb_3 molecules,[15,19] chemical access to these highly complex glycolipids is a challenging and time-consuming endeavour. Nevertheless, such a synthetic approach is the method of choice to gain chemically pure material which is needed for proper biophysical investigations. In 2007, Florent and co-workers already devised a synthetic route from the trisaccharidic subunit to Gb_3-C22:0 and Gb_3-C22:1 glycosphingolipids.[6]

In this paper, we describe a generally applicable and modular strategy to assemble the target glycosphingolipids starting from simple monosaccharide building blocks, sphingosine and fatty acids. Saturated, unsaturated, α-hydroxylated fatty acids and a combination thereof were employed. These molecules were reconstituted into membranes composed of sphingomyelin, cholesterol, and 1,2-dioleoyl-*sn*-glycero-3-phosphocholine (DOPC) resembling the composition of the outer leaflet of animal plasma membranes and that are known to phase-separate.[20,21] Solid supported membranes (SSMs) in conjunction with fluorescence microscopy and atomic force microscopy were used to investigate the lateral organization of the membranes as a function of Gb_3 composition and STxB binding. Despite a reduced lateral lipid mobility found in SSMs, these membranes are sufficiently dynamic to allow for lipid rearrangement while offering the possibility to use fluorescence microscopy and high resolution atomic force microscopy (AFM) to monitor nanometre-sized domains.[22,23] We provide evidence that the fatty acid strongly influences the phase behaviour of the membranes as well as the mode of STxB cluster formation.

Results

Synthesis of Gb_3 glycosphingolipids

The power of a synthetic approach towards Gb_3 glycosphingolipids is most promising due to the highly defined nature of the obtained material. From a retrosynthetic point of view a glycosphingolipid can be divided into three major parts: (i) the carbohydrate head group as the hydrophilic and the ceramide as the lipophilic part that can be further subdivided into (ii) a sphingosine such as D-*erythro*-sphingosine and (iii) a fatty acid being attached to the amine of the sphingosine (Scheme 1). We assembled four different glycosphingolipids, which consist of the globotriaose head group, the sphingosine, but differ in the fatty acid chain. Saturated, unsaturated, α-hydroxylated derivatives and a combination thereof were prepared, all based on a C_{24} fatty acid. C_{24} fatty acids have been chosen as they are the major constituent (>50%, ESI†) found in natural Gb_3 mixtures such as toxin insensitive erythrocytes,[14] HeLa-cells,[24] and HEp-2 cells.[25]

The globotriaoside is traced back to three different monosaccharide building blocks (Scheme 1, **1**–**3**). Glucose derivative **1** was obtained in four steps starting from 3,6-di-*O*-benzyl-D-glucal[26] being an ideal precursor for various glucose-derived building blocks. Fmoc protection of the 4-*O*-hydroxyl group followed by epoxidation with dimethyldioxirane (DMDO)[27] and epoxide opening using benzylic alcohol led to a glucose derivative with a free hydroxyl group in C-2 position. Acetylation and Fmoc removal provided glucosyl acceptor **1** (ESI†). Galactosyl building block **2** was synthesized starting from 3,6-di-*O*-benzyl-D-galactal (**10**).[28] Fmoc protection of the free hydroxyl and subsequent epoxidation with DMDO followed by epoxide opening with dibutyl phosphate terminated by pivaloyl protection of the emerging 2-hydroxyl afforded building block **2** (ESI†).[29] The third unit, an α-linked galactose, was prepared

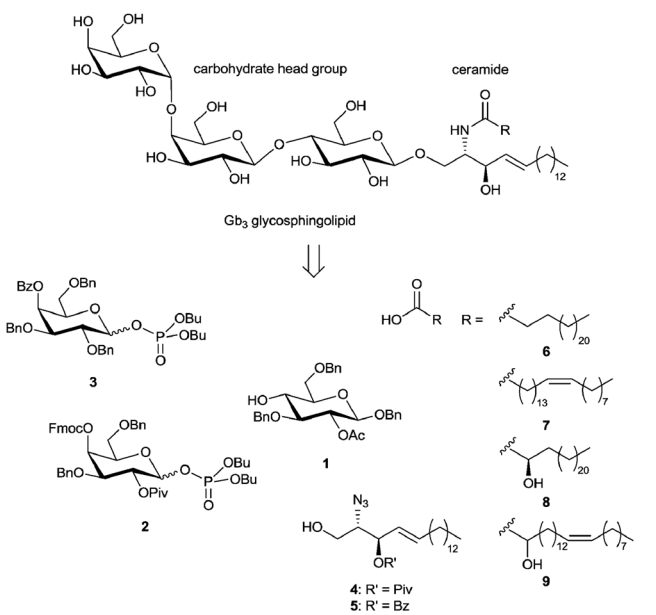

Scheme 1 Retrosynthetic analysis of Gb_3 glycosphingolipids.

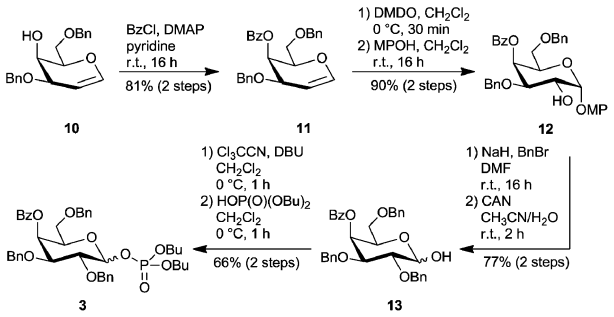

Scheme 2 Preparation of α-galactosyl building block **3**.

starting from **10** as well (Scheme 2). To facilitate the formation of the α-galactosidic linkage in the trisaccharide a remote-participating group (Bz)[30] was installed at the 4-hydroxyl of **10**. DMDO-mediated epoxidation of galactal **11** and attack with *p*-methoxyphenol (MPOH) led to acetal **12** in 90% yield. Benzyl ether formation and removal of the anomeric protecting group under oxidative conditions furnished hemiacetal **13**.

The latter was first converted into a trichloroacetimidate[31] and subsequently transformed to phosphate **3** which proved to be more suitable in this glycosylation reaction than the trichloroacetimidate analogue.

With these monosaccharide building blocks in hand we started the assembly of the globotriaose. The sequence commences with the union of building blocks **1** and **2** using TMSOTf as Lewis acidic promoter (Scheme 3). The β-selectivity is ensured due to neighbouring group participation of the pivaloate of galactose building block **2**. Subsequent removal of the Fmoc protecting group under mild basic conditions followed by the second glycosylation with building block **3** led to trisaccharide **14** in 79% yield (over three steps) and pure α-selectivity as it was anticipated by the remote participation[30] of the benzoyl protecting group at C-4. In addition, a reaction temperature of −60 °C proved to be beneficial as well to achieve complete diastereoselectivity. In case of the more reactive per-benzylated galactosyl phosphate both, the yield and the selectivity, dramatically dropped down.

The commonly used technique to deprotect the permanent benzyl protecting groups by hydrogenolysis at the very end of an oligosaccharide synthesis is not a choice in the assembly of glycosphingolipids since their double bond would be destroyed during such a reduction step. Thus, the protecting groups of the globotriaose unit had to be exchanged before the union with the lipid part takes place. Taking these difficulties into account, benzoyl groups being easily cleaved under basic conditions were installed. In order to get perbenzoylated material, firstly, the three different acyl groups were removed under strong basic conditions, followed by a hydrogenolysis of the benzyl ethers using Pearlman's catalyst. Perbenzoylation of the naked trisaccharide was performed followed by removal of the anomeric benzoate using methylamine. Finally, a trichloroacetimidate moiety was installed as leaving group to yield globotriaoside derivative **17** in 99% yield.

In addition, two hydroxylated fatty acids being not commercially available had to be prepared. Based on a route developed by Kiso, Ando and co-workers, α-hydroxylated tetracosanoic acid **22** was generated (Scheme 4a).[32] Alkyne **18**, readily available from 1-eicosanol, was used to open epoxide **19**. The secondary hydroxyl group was directly protected with a benzoyl group to afford **20** in 45% yield over two steps. Hydrogenation using palladium on charcoal furnished the saturated debenzylated alkane chain whereas Pearlman's catalyst induced an acyl group migration. Finally, the primary hydroxyl group of **21** was oxidized to fatty acid **22** in 73% yield using TEMPO/TCCA

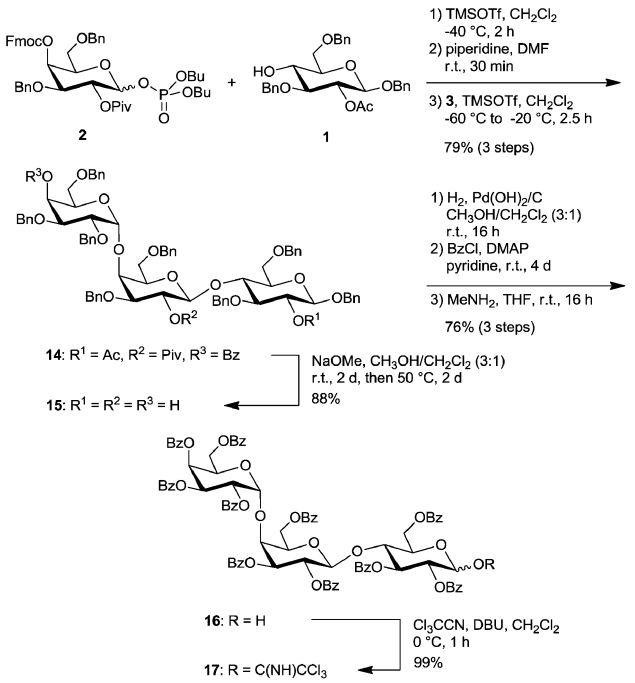

Scheme 3 Assembly of the globotriaosyl trichloroacetimidate **17**.

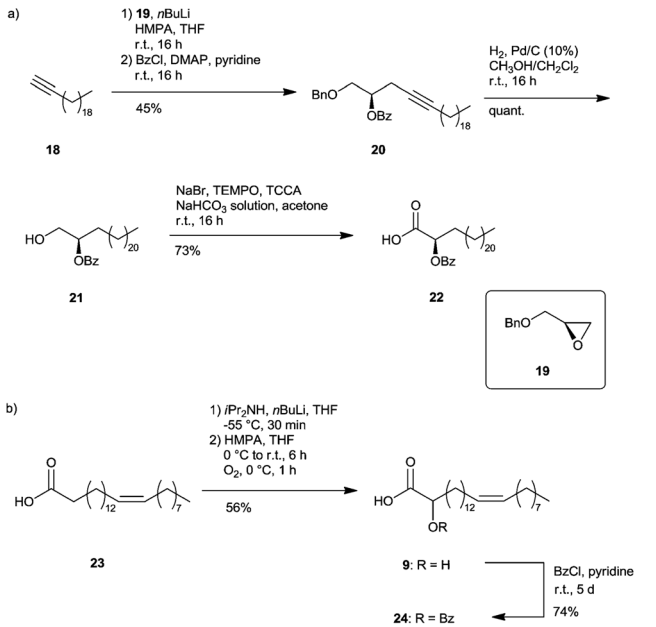

Scheme 4 Syntheses of hydroxylated fatty acids **22** and **24**.

conditions. The protected α-hydroxylated nervonic acid **24** was synthesized starting from nervonic acid in two steps (Scheme 4b).

After carboxylate enolate formation using freshly prepared LDA, a dry oxygen atmosphere attached to the reaction, derivatised the α-position with a hydroxyl group to yield **9** in 56%.[33] Final benzoylation of this secondary hydroxyl gave the desired fatty acid **24**. To complete total synthesis, globotriaosyl trichloroacetimidate **17** and the protected sphingosine **4** or **5**,[34] respectively, were coupled in a glycosylation reaction using $BF_3 \cdot OEt_2$ to afford **25** or **26**, in moderate yields (Scheme 5). In case of the benzoyl protected sphingosine only a minor acyl group migration was observed. Staudinger reduction of the azide and direct coupling with the fatty acids **6–9** under peptide coupling conditions (*e.g.* HATU or HOBt/EDCI)[35] led to four protected glycosphingolipids, varying in their acyl chains. Global deprotection under Zemplén conditions resulted in the desired glycosphingolipids **27–30**.

Phase behaviour of solid supported membranes doped with different Gb_3s

SSMs that separate into a liquid-ordered (l_o) and liquid-disordered (l_d) phase at room temperature were obtained by spreading unilamellar vesicles composed of the well-established lipid mixture DOPC/sphingomyelin (SM)/cholesterol (Chol) in a molar ratio of 2 : 2 : 1 on mica surfaces.[36] Vesicle spreading was achieved at elevated temperatures (55 °C) above the phase-transition temperature of the lipid mixture ($T_m \approx 40$ °C).[37] At room temperature, the membrane is phase-separated into a l_o and a l_d phase, as can be revealed from fluorescence micrographs (ESI, Fig. S1A†) using sterically demanding fluorophors (Bodipy-PC, Texas Red DHPE, Oregon Green DHPE) that preferentially partition into the l_d phase.[38] The overall membrane integrity was verified for each experiment using the dye perylene, which distributes more equally between the l_o and l_d phase (ESI, Fig. S1B†). The percentage of the l_o phase was determined by pixel analysis to be 66 ± 6% ($n = 35$). To this lipid mixture, the globotriaosylceramide Gb_3 serving as the receptor lipid for STxB was added by replacing 5 mol% of the used bovine brain SM (ESI, Table S2†). This exchange retains the principal l_o/l_d phase-separation of the membranes.[9] To scrutinize the influence of the fatty acid of Gb_3 on the phase behaviour of the SSMs, one of the four synthesized Gb_3 molecules (**27–30**) were incorporated into the phase-separated membranes. Besides the Gb_3 with the C24:0 fatty acid (**27**, Gb_3-C24:0), we analysed the influence of the α-hydroxylated fatty acid (**29**, Gb_3-C24:0-2OH), an unsaturated fatty acid (**28**, Gb_3-C24:1), as well as both, an unsaturated and α-hydroxylated fatty acid (**30**, Gb_3-C24:1-2OH).

Characteristic fluorescence images of a solid supported membrane composed of DOPC/SM/Chol/Gb_3 (40 : 35 : 20 : 5)

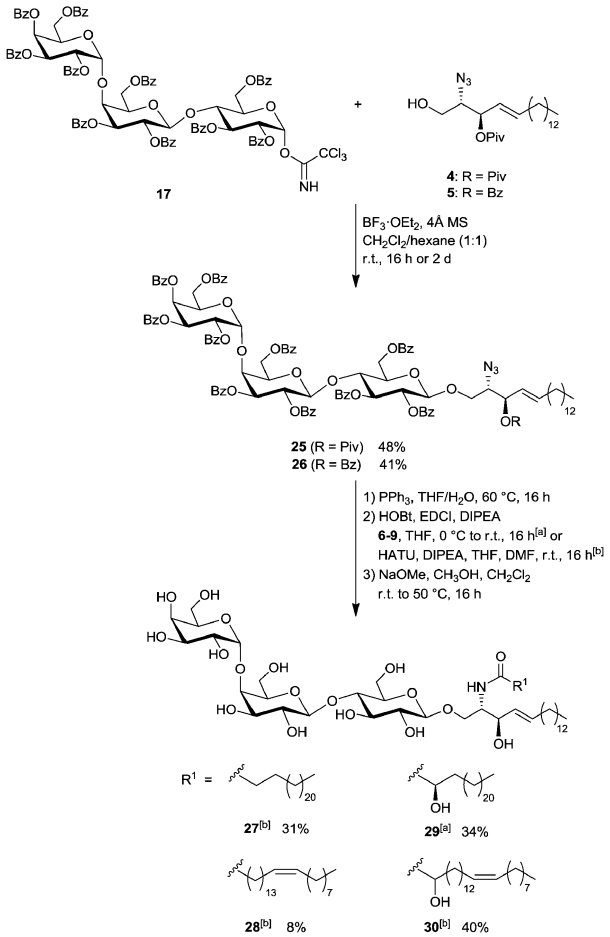

Scheme 5 Gb_3 glycosphingolipid assembly.

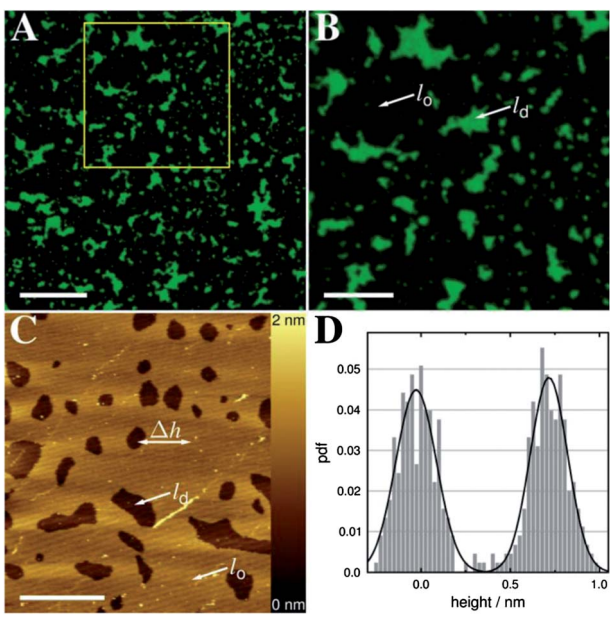

Fig. 1 SSMs composed of DOPC/SM/Chol/Gb_3-C24:0 (40 : 35 : 20 : 5) doped with perylene (0.5 mol%) and Texas Red DHPE (0.1 mol%) on mica. (A) Fluorescence micrograph of Texas Red DHPE (false coloured in green). Membranes segregate into liquid-ordered (l_o, dark) and liquid-disordered domains (l_d, green). Scale bar: 20 μm. (B) Magnification of the region marked in (A). Scale bar: 10 μm. (C) AFM image showing a higher l_o phase and a lower l_d phase (darker colour coding). Scale bar: 5 μm. (D) Histogram analysis showing a height difference $\Delta h(l_o/l_d) = 0.7 \pm 0.2$ nm for the image shown in (C).

with Gb_3-C24:0 are shown in Fig. 1A and B. The fluorescence of Texas Red DHPE (false coloured in green) indicates the l_d phase, while the dark areas are attributed to the l_o phase, which excludes the fluorescent lipid. The area percentage of the l_o phase was determined by pixel analysis and amounts to 74 ± 7% ($n = 84$). By means of atomic force microscopy (AFM), the topography of the phase-separated membranes was analysed (Fig. 1C). Domains of lower height are visualized in the AFM image, which are assigned to the l_d phase (darker colour coding) embedded in a higher l_o phase. The height difference between the l_o and l_d phase was determined by histogram analysis (Fig. 1D) to be $\Delta h(l_o/l_d) = 0.6 \pm 0.2$ nm ($n = 21$) in agreement with height differences reported in literature.[39]

For membranes containing 5 mol% of Gb_3-C24:0-2OH (ESI, Fig. S2†), again a phase-separated lipid membrane was visualized in fluorescence microscopy as well as in atomic force microscopy, from which the l_o and l_d phase could be unambiguously assigned with a typical height difference of $\Delta h(l_o/l_d) = 0.8 \pm 0.1$ nm ($n = 87$). However, the area percentage of the l_o phase was, with 56 ± 5% ($n = 56$), significantly lower compared to the lipid mixture containing 5 mol% of Gb_3-C24:0. Given the fact that only the 5 mol% component Gb_3 was replaced in the lipid mixture, while all other lipid components remained constant, a change of about 20% of the area percentage of the l_o phase was rather unexpected suggesting a more global impact of the Gb_3 molecules on the phase-separation behaviour of the membrane as discussed in more detail below.

Surprisingly different phase behaviour was observed if the lipid mixture contained Gb_3-C24:1. The fluorescence micrographs of Texas Red DHPE show three fluorescence intensities (Fig. 2A and B). While a bright green phase is still clearly visible and can be identified by the enrichment of the fluorescent dye, a dark phase as well as a phase with an intermediate brightness is observed. We assign the membrane phase, from which Texas Red DHPE is mostly excluded to the l_o phase, while the phase with the highest fluorescence intensity is attributed to the l_d phase. The phase of intermediate brightness is termed l_i phase and was found independently of the l_d marker dye used (ESI†). According to this assignment, one can determine the area percentages of all three phases ($n = 73$) being for the l_d phase 23 ± 6%, for the l_i phase 36 ± 8% and for the l_o phase 40 ± 6%. By atomic force microscopy, only in rare cases the three phases were resolved by their differences in height (Fig. 2C). In case of the detection of three different height levels we assigned the lowest one to the l_d phase. As it is not possible to assign the l_i phase and the l_o phase to the different heights in the AFM images, we took the l_d phase as the reference and determined two height differences with $\Delta h_1 = 1.2 \pm 0.2$ nm ($n = 4$) and $\Delta h_2 = 1.6 \pm 0.2$ nm ($n = 5$). In several AFM images, the two different heights could not be resolved resulting in an averaged value of $\Delta h_{1/2} = 1.2 \pm 0.2$ ($n = 68$).

For Gb_3-C24:1-2OH, which contains the *cis*-double bond as well as the hydroxylation in the 2-position, the membrane again only separated into two phases assigned to as l_d and l_o with an area percentage of 70 ± 7% ($n = 51$) resembling the situation of Gb_3-C24:0 more than the other Gb_3 species. Table 1 summarizes the area percentages found for the different Gb_3 molecules as well as the height differences between the observed lipid phases as deduced from AFM analysis in the otherwise identical lipid mixtures.

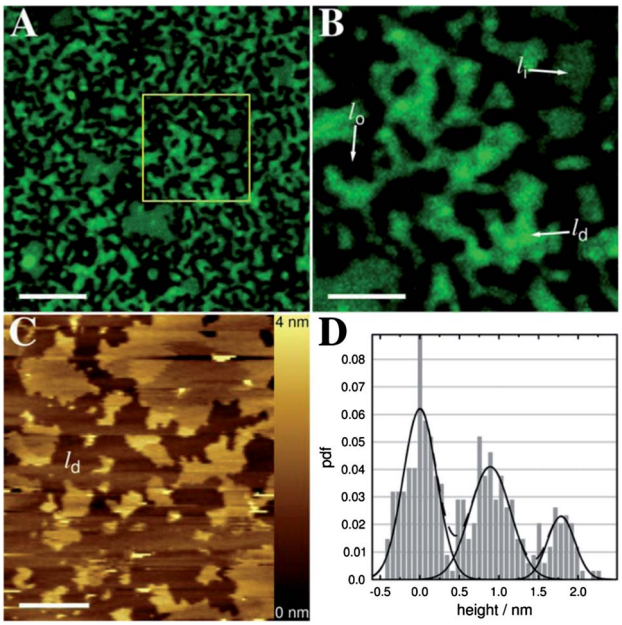

Fig. 2 SSMs composed of DOPC/SM/Chol/Gb_3-C24:1 (40 : 35 : 20 : 5) doped with perylene (0.5 mol%) and Texas Red DHPE (0.1 mol%). (A) Fluorescence micrograph of Texas Red DHPE (false coloured in green). Membranes segregate into three phases as indicated by three brightness levels. Scale bar: 10 μm. (B) Magnification of the region marked in (A). Additionally to liquid-ordered (l_o, dark) and liquid-disordered domains (l_d, bright green) a third lipid phase of intermediate brightness (l_i) is identified. Scale bar: 4 μm. (C) AFM image showing the three phases. While the lowest phase is assigned to the l_d phase, the two other phases differing in height cannot be unambiguously assigned to the l_o and l_i phase. Scale bar: 2 μm. (D) Histogram analysis showing the heights of the three phases. Taking the l_d phase as the lowest phase, two height differences of $\Delta h_1 = 0.9 \pm 0.4$ nm and $\Delta h_2 = 1.8 \pm 0.4$ nm are calculated for the image shown in (C).

Table 1 Ratios of the different membrane phases (l_o: liquid-ordered, l_i: liquid-intermediate) in DOPC/SM/Chol/Gb_3 (40 : 35 : 20 : 5) bilayers doped with different Gb_3s on mica and height differences observed in AFM images. The ratios were determined by pixel analysis using fluorescence images. Height differences were extracted by fitting Gaussians to the height histograms. For compound **27**, **29**, and **30** Δh_2 corresponds to the height difference between l_o and l_d phase ($\Delta h(l_o/l_d)$) (number of analysed fluorescence images and height histograms is given in brackets)

Compound	l_o/%	l_i/%	Δh_2/nm	Δh_1/nm
27	74 ± 7 (84)	—	0.6 ± 0.2 (21)	—
28	40 ± 6 (73)	36 ± 8	1.6 ± 0.2 (5)	1.2 ± 0.2 (4)
29	56 ± 5 (56)	—	0.8 ± 0.1 (87)	—
30	70 ± 7 (51)	—	0.5 ± 0.2 (31)	—

Our findings demonstrate that the fatty acid composition of the glycosphingolipid Gb_3 strongly influences the phase behaviour of the phase-separated lipid membranes, even though it amounts only to 5 mol% of the whole lipid

composition. This result implies that Gb_3 strongly interacts with the other lipid components thus altering the phase behaviour.

STxB binding to solid supported membranes doped with different Gb_3s

The B-subunits of the protein Shiga toxin are known to alter the phase behaviour of membranes, when they bind to their receptor lipid Gb_3.[9,10,40] We thus elucidated the impact of STxB binding on the phase behaviour of the lipid mixture containing different Gb_3 species by using fluorescently labelled STxB. In l_o/l_d phase-separated membranes containing a mixture of different Gb_3 species, it has been shown that the Gb_3s are located in the l_o phase after STxB binding.[9] The position of the protein fluorescence therefore allows us to localize the Gb_3 molecules after protein binding. After preparation of SSMs composed of DOPC/SM/Chol/Gb_3 (40 : 35 : 20 : 5) on mica containing one of the four different Gb_3 species, they were incubated with 60 nM of STxB for 1 h, rinsed with buffer and inspected by fluorescence microscopy. The fluorescent lipid Texas Red DHPE was exchanged against Oregon Green DHPE or Bodipy-PC, which also label the l_d phase, to be able to monitor the l_d phase (green) at the same time as the fluorescence of the Cy3-labeled STxB (red). Control experiments reveal that non-specific binding of STxB to DOPC/SM/Chol (2 : 2 : 1) membranes lacking Gb_3 can be neglected.

For Gb_3-C24:0 containing membranes, the Oregon Green DHPE micrographs show phase-separated membranes with l_o phase and l_d phase after STxB binding (Fig. 3A). The corresponding Cy3-fluorescence image of the bound STxB shows inverse fluorescence, indicating that the protein has been bound to the l_o phase, in which the Gb_3 molecules are located (Fig. 3B). The area percentage of the l_o phase does not change upon protein binding (76 ± 11%, $n = 52$). From the STxB-Cy3 fluorescence image as well as from the AFM images, it becomes obvious that the protein does not homogeneously bind to the l_o phase but forms clusters. The height difference between the protein clusters on the l_o phase and the overall height of protein-decorated l_o-phase is $\Delta h(l_{o+STxB\_clusters}/l_{o+STxB}) = 0.8 \pm 0.1$ nm ($n = 6$). The overall increase in height of the l_o phase in the presence of bound protein is only very minor with an increase of $\Delta h(l_{o+STxB}/l_d) - \Delta h(l_o/l_d) = 0.1 \pm 0.4$ nm indicating that the protein surface coverage on the entire l_o phase is, except for the dense protein domains, rather low.

Phase-separated membranes containing Gb_3-C24:0-2OH with considerably reduced area percentage of the l_o phase prior to protein binding of only 56 ± 5%, experience a significant increase in l_o phase after STxB binding (77 ± 5%, $n = 62$). The STxB-Cy3 fluorescence is inhomogeneous (ESI, Fig. S3†)

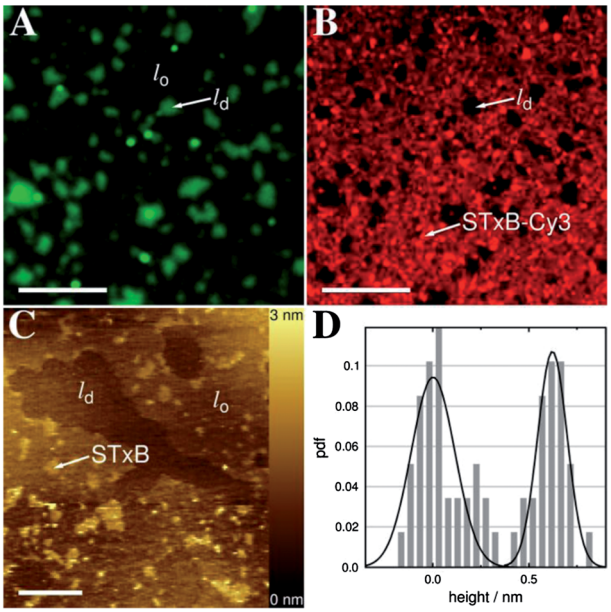

Fig. 3 SSMs composed of DOPC/SM/Chol/Gb_3-C24:0 (40 : 35 : 20 : 5) doped with perylene (0.5 mol%) and Oregon Green DHPE (0.1 mol%) after incubation with 60 nM Cy3-labeled STxB. (A) Fluorescence micrograph of Oregon Green DHPE. Membranes segregate into l_o (dark) and l_d (green) domains. Scale bar: 15 μm. (B) Fluorescence micrograph of STxB-Cy3. The inhomogeneous red fluorescence of the labeled protein is inverse to the Oregon Green DHPE labeled l_d phase. Scale bar: 15 μm. (C) AFM image showing a lower l_d phase (dark colour coding), higher l_o phase and STxB clusters on top of the ordered phase. Scale bar: 2 μm. (D) Height difference between STxB clusters and protein decorated l_o phase is determined to $\Delta h(l_{o+STxB\_clusters}/l_{o+STxB}) = 0.6 \pm 0.2$ nm for the image shown in (C).

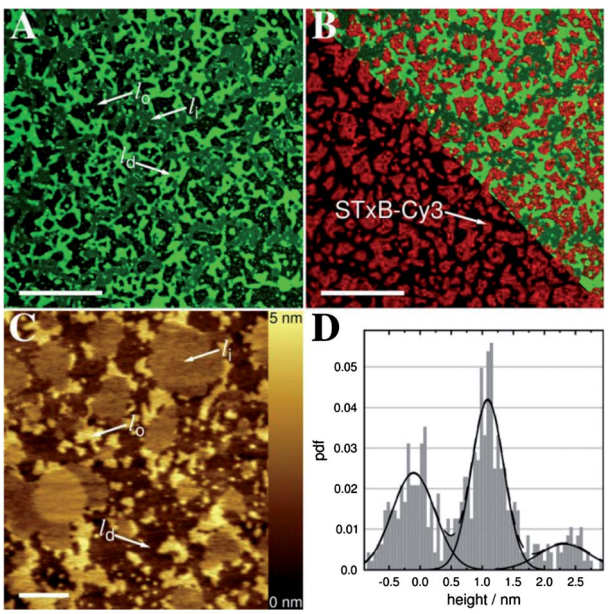

Fig. 4 SSMs composed of DOPC/SM/Chol/Gb_3-C24:1 (40 : 35 : 20 : 5) doped with perylene (0.5 mol%) and Bodipy-PC (0.1 mol%) after incubation with 60 nM Cy3-labeled STxB. (A) Fluorescence micrograph of Bodipy-PC. The membrane segregates into three phases as indicated by three brightness levels. Scale bar: 15 μm. (B) Fluorescence of Cy3-labeled STxB shows protein binding to the l_o phase. Top right corner: overlay with Bodipy-PC fluorescence. Scale bar: 15 μm. (C) AFM image of the bilayer after STxB incubation. Three different height levels are observed. Scale bar: 2 μm. (D) Histogram analysis of the heights of the three phases. Taking the l_d phase as the lowest phase, where no protein has been bound to, two height differences of $\Delta h(l_i/l_d) = 1.2 \pm 0.8$ nm and $\Delta h(l_{o+STxB}/l_d) = 2.4 \pm 0.8$ nm are calculated.

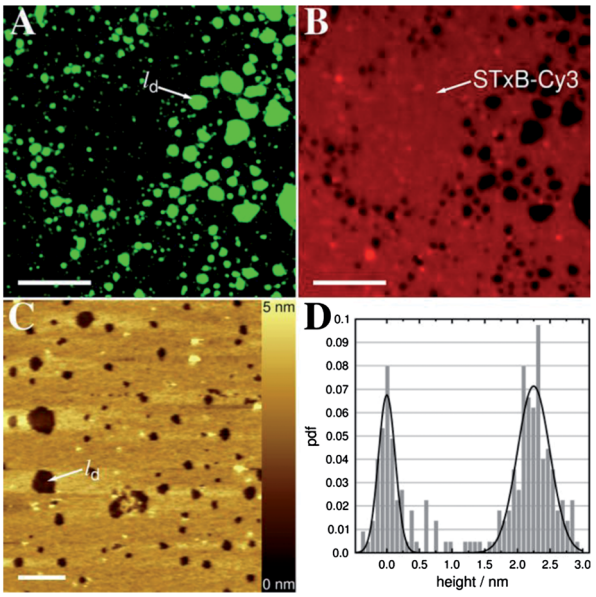

Fig. 5 SSMs composed of DOPC/SM/Chol/Gb_3-C24:1-2OH (40 : 35 : 20 : 5) doped with perylene (0.5 mol%) and Oregon Green DHPE (0.1 mol%) after incubation with 60 nM Cy3-labeled STxB. (A) Fluorescence micrograph of Oregon Green DHPE. The membrane segregates into a l_o (dark) and l_d (green) phase. Scale bar: 15 μm. (B) Fluorescence micrograph of the STxB-Cy3 fluorescence. STxB is only located on the l_o domains. Scale bar: 15 μm. (C) AFM image showing the higher l_o phase and a lower l_d phase (darker colour coding). Scale bar: 2 μm. (D) Height difference between the two identified phases in the histogram with $\Delta h(l_{o+STxB}/l_d) = 2.3 \pm 0.5$ nm.

indicating protein cluster formation. The AFM images resolve STxB clusters on the protein-decorated l_o phase with $\Delta h(l_{o+STxB\_clusters}/l_{o+STxB}) = 0.7 \pm 0.2$ nm ($n = 24$). In addition, the overall height of the l_o phase as a result of protein binding increases only by 0.2 nm to $\Delta h(l_{o+STxB}/l_d) = 1.0 \pm 0.2$ nm ($n = 69$) indicating low protein density (ESI, Fig. S3†).

Membranes containing Gb_3-C24:1 are quite distinct from the other Gb_3-containing membranes as they phase-separate into three different phases. Upon STxB binding, the overall phase-separation did not change. Fig. 4A depicts a Bodipy-PC fluorescence micrograph again showing three different intensities. The disordered phase is assigned to the bright green fluorescent phase, the intermediate phase to that with the lower fluorescence intensity and the dark one to the ordered phase.

Fig. 4B shows the localization of Cy3-labeled STxB. Interestingly, the protein only binds to one of the three phases, namely to the assigned l_o phase. This in turn would imply that after STxB binding, the Gb_3 receptors are located only in the l_o phase. The area percentages of the phases do not change upon STxB binding being 43 ± 7% and 31 ± 8% for the l_o and l_i phase, respectively. However, in contrast to the other Gb_3 containing membranes, the domain morphology changes considerably, *i.e.* all domains condense into larger ones. The height difference of $\Delta h(l_i/l_d) = 1.3 \pm 0.7$ nm ($n = 12$) corresponds to the height difference between the l_d phase and the non-protein covered l_i phase. The rather large difference between the l_d and l_i phase might be interpreted in a sense that the l_i phase is highly ordered, composed of mostly saturated lipids. The protein bound to the Gb_3 containing l_o phase results in a height difference of $\Delta h(l_{o+STxB}/l_d) = 2.6 \pm 0.6$ nm ($n = 26$).

For membranes containing Gb_3-C24:1-2OH, two phases are identified with the l_o phase being visualized by the red STxB-Cy3 fluorescence (Fig. 5A and B). Of note, in accordance with the observation made for the saturated, α-hydroxylated compound Gb_3-C24:0-2OH, the area fraction of the l_o phase is significantly increased from 70 ± 7% to 87 ± 7% ($n = 42$).

This result implies that more DOPC molecules are recruited into the lipid dye excluding phase. In contrast to the other Gb_3 derivatives under investigation, the topography mapped by AFM (Fig. 5C) only shows two height levels with a height difference of $\Delta h(l_{o+STxB}/l_d) = 2.7 \pm 0.5$ nm ($n = 44$).

The higher phase is the l_o phase with bound protein as deduced from the fluorescence images. No individual proteins can be resolved, however the increase in height as a result of protein binding amounts to $h_{STxB} = \Delta h(l_{o+STxB}/l_d) - \Delta h(l_o/l_d) = 2.2 \pm 0.7$ nm, which indicates a high protein density on the surface resulting in a thickness that matches the crystallographic dimensions of STxB.[41]

Table 2 summarizes the properties observed in fluorescence microscopy and atomic force microscopy after STxB binding to the membranes.

Discussion

There are several lines of evidence that membrane bending leading to the observed Shiga toxin invaginations in cells and GUVs are preceded by a local compaction of lipids in one leaflet leading to an asymmetric reduction in membrane area.[9,11] Such local lipid compaction is accompanied by protein cluster formation and lipid sorting.[9,40] On the other hand, protein binding studies suggest that the binding capacity of a

Table 2 Ratios of the different membrane phases (l_o: liquid-ordered, l_i: liquid-intermediate) in DOPC/SM/Chol/Gb_3 (40 : 35 : 20 : 5) bilayers doped with different Gb_3s on mica and height differences observed in AFM images after STxB binding. The ratios were determined by pixel analysis using fluorescence images. Height differences were extracted by fitting Gaussians to the height histograms (number of analysed fluorescence images and height histograms is given in brackets)

Compound	l_o/%	l_i/%	$\Delta h(l_i/l_d)$/nm	$\Delta h(l_{o+STxB\_clusters}/l_{o+STxB})$/nm	$\Delta h(l_{o+STxB\_clusters}/l_d)$/nm	$\Delta h(l_{o+STxB}/l_d)$/nm	$\Delta h(l_{o+STxB}/l_i)$/nm
27	76 ± 11 (52)	—	—	0.8 ± 0.1 (6)	1.5 ± 0.5 (19)	0.7 ± 0.2 (17)	—
28	43 ± 7 (64)	31 ± 8	1.3 ± 0.7 (12)	—	—	2.6 ± 0.6 (26)	1.9 ± 0.6 (15)
29	77 ± 5 (62)	—	—	0.7 ± 0.2 (24)	2.1 ± 0.5 (12)	1.0 ± 0.2 (69)	—
30	87 ± 7 (42)	—	—	—	—	2.7 ± 0.5 (44)	—

membrane for STxB depends on the fatty acid of Gb_3.[15,19,41] Thus, we asked the question whether protein cluster formation and lipid sorting leading to local lipid compaction is altered by the fatty acid composition of Gb_3, which would then have great impact on the propensity of a membrane to invaginate as a result of STxB binding. We will first discuss the individual observations made with the four synthetically derived Gb_3 molecules, which sum up to more than 50% of the Gb_3s found in natural mixtures,[14,24,25] and then discuss the impact on STxB cluster formation and toxin invasion.

In case of Gb_3-C24:0 with a long chain saturated fatty acid, the assigned l_o phase amounts to 74% of the total membrane area. Incubation with STxB did not alter this percentage indicating that no gross lipid reorganization between the two phases takes place. We suggest that the Gb_3 molecules are preferentially localized in l_o domains with the saturated fatty acid chain interacting with cholesterol resulting in a tightly packed l_o phase before as well as after STxB binding (Fig. 6).

The lipid mixture containing Gb_3-C24:0-2OH exhibits about 20% less ordered phase (56% area fraction of l_o phase) under the same experimental conditions before protein addition and thus suggests that the l_o phase is mainly composed of the sphingolipids and cholesterol, which would sum up to a theoretical area fraction of about 50%,[42] if one takes only the geometry of the lipid molecules into account (ESI†). However, after STxB binding the area percentage of the l_o phase increases significantly to 77%. It has been shown by others that acyl chain hydroxylation only slightly changes the transition temperature of ternary lipid mixtures but affects the interlipid interaction, *e.g.* attenuates the interaction with sterols leading to a fluidization of the bilayer.[16] This implies that part of the DOPC molecules has been relocated from the l_d to the l_o phase upon protein binding. In a similar fashion, the area percentage of membranes containing Gb_3-C24:1-2OH increases by roughly 20% upon protein binding. Scheve *et al.*[43] reported that, owing to the sterical demand of a protein to bind to its receptor, it

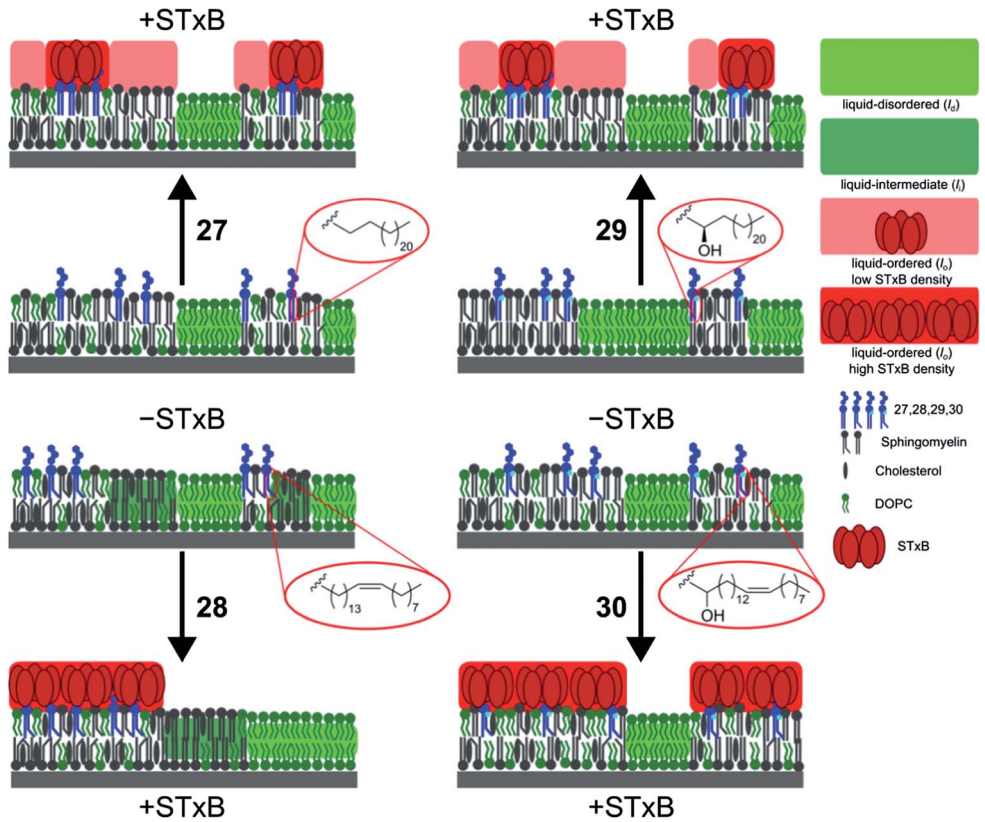

Fig. 6 Schematic drawing of the phase behaviour of lipid membranes induced by different Gb_3 species in absence and presence of STxB. For simplicity, Gb_3 molecules have only been drawn in the upper leaflet of the bilayer. The localization of the Gb_3s prior to protein binding is only hypothesized. (**27**) Membranes doped with Gb_3-C24:0 segregate into l_o and l_d phase with an l_o phase area percentage of more than 70%. Binding of STxB does not lead to lipid redistribution between the phases. After STxB binding Gb_3 is located in the l_o phase and STxB demixes the l_o phase by clustering the Gb_3 leading to STxB clusters. (**29**) Membranes doped with Gb_3-C24:0-2OH exhibit a low l_o area percentage due to a presumably tight lipid packing excluding DOPC. STxB binding recruits and clusters Gb_3 in the ordered phase leading to protein clusters. Additionally, the l_o phase area percentage is increased indicating that Gb_3 recruitment allows for inclusion of DOPC in the l_o phase. (**30**) Prior to protein binding membranes containing Gb_3-C24:1-2OH show a similar behaviour as described for **27**. Interestingly, protein binding again leads to a strong increase of the l_o phase area fraction. The high protein density atop the l_o phase indicates steric pressure between proteins bound to the receptor lipids inducing a mixing of the phases.[43] (**28**) Gb_3-C24:1 induces a demixing of the membrane in absence of protein resulting in a third intermediate phase differing in height and fluorophore partition. STxB selectively binds only to one of the three phases showing that Gb_3-C24:1 is solely located in this phase.

induces an increased lipid mixing eventually leading to the disruption of l_o/l_d phase separation, a phenomenon that could also explain the gross relocalization of DOPC from the l_o to the l_d phase upon STxB binding.

Unsaturated Gb_3 induces a visible demixing of the ordered phase, which we termed l_i and l_o phase according to their fluorescence intensities in the fluorescence images. Just recently, Sodt *et al.*[44] reported on substructures within the liquid-ordered phase of lipid bilayers as obtained by molecular dynamics simulations. These substructures, identified in a 10 μs all-atom trajectory of l_o/l_d coexistence were composed of saturated hydrocarbon chains packed with local hexagonal order and separated by interstitial regions enriched in cholesterol and unsaturated chains. In our case, the unsaturated Gb_3 molecules might foster such demixing of the l_o phase interacting preferentially with the unsaturated species of bovine brain sphingomyelin (ESI, Table S2†) and cholesterol and separate from the saturated species of bovine brain sphingomyelin.[45] Even though the molecules are unsaturated, it is expected that they still exclude the bulky fluorophore, as it has been shown in monolayer experiments that ceramides with an unsaturated fatty acid tightly pack despite their large steric demand.[46] As there is not only a difference in fluorophore partition between the two observed phases but also a height difference as obtained by AFM images, we suggest that Gb_3-C24:1 is localized only in one of the two phases thus increasing the height owing to the size of the Gb_3 head group.[47] We cannot unambiguously decide whether the l_i or l_o phase in the fluorescence micrographs contains the Gb_3, as the area percentage of the domains are similar but given the percentage of l_d phase (24% for Gb_3-C24:1 compared to 26% for Gb_3-C24:0) we assume the two phases to be the result of segregation of the l_o phase.

Using the phase diagram and tie-lines gathered from fluorescence micrographs of GUVs reported by Bezlyepkina *et al.*,[42] one can estimate the compositions and area fractions of the l_o and l_d phases. In general, the area fraction we found for the l_d phase in our SSMs composed of DOPC/SM/cholesterol (2 : 2 : 1) is lower than that found for GUVs (63%), which probably reflects the influence of the solid support (ESI†). Despite this general trend, we found that independent of whether we theoretically replace either 5 mol% of SM or DOPC with 5 mol% of unsaturated Gb_3 in the DOPC/SM/cholesterol (2 : 2 : 1) lipid mixture, this does not explain the observed changes in l_d area fraction suggesting that the Gb_3 influences also the surrounding lipids (ESI, Fig. S5†). We expect to observe the same behaviour when using 1-palmitoyl-2-oleoyl-*sn*-glycero-3-phosphocholine bearing one saturated and one unsaturated fatty acid chain instead of DOPC as the general phase behaviour is very similar,[37,48] even though POPC can stabilize nanoscopic domains.[49]

After STxB binding, a change in lateral membrane organization as well as protein cluster formation was expected. However, in contrast to our previous study,[9] where we used a Gb_3 mixture, protein cluster formation as well as membrane reorganization strongly depended on the used Gb_3 molecule. We found that STxB binds to the l_o phase demonstrating the localization of the different Gb_3s with the sphingomyelin/cholesterol enriched phases regardless of the fatty acid attached to the molecule.[40,50] Membranes containing Gb_3 with a saturated fatty acid show densely packed protein clusters surrounded by less compact bound STxB. In contrast, STxB binds rather homogeneously and with high density to the l_o phase of membranes containing Gb_3 with an unsaturated fatty acid. This result might be correlated with the finding that the membrane binding capacity for STxB is larger in case of unsaturated Gb_3s.[15,19] Given the affinity constants of STxB to Gb_3, all binding sites on the membrane are expected to be occupied.[13] However, the number of Gb_3 molecules bound to a STxB pentamer might vary for the different Gb_3-doped membranes. From the crystal structure of STxB co-crystallized with a soluble receptor analogue, it is known that up to 15 Gb_3 molecules can bind to the pentamer resulting in dense packing of the receptor lipids.[41,51] If a large number of Gb_3s is bound to the STxB pentamer, the membrane gets depleted in Gb_3 resulting in localized protein clusters rather than in a homogeneously covered membrane surface. As a lower limiting case, we assumed that all 15 binding sites of STxB are occupied with Gb_3, which would result in a theoretical protein surface coverage of roughly 16% (ESI†). From the AFM images (Fig. 3C), we estimated a 15% surface coverage for the STxB clusters on Gb_3-C24:0 containing membranes, which is in a similar range as the theoretically estimated value. However, as there are also proteins bound to the membrane but not in clusters, one can state that the number of Gb_3 molecules bound per STxB is less than 15 but probably very high. Receptor clustering as a result of toxin binding was also described for Cholera toxin subunit-B resulting in less protein surface coverage at higher G_{M1} concentrations.[52] In contrast, the unsaturation of the fatty acid in Gb_3 increases the area demand of this molecule, which might decrease the number of Gb_3s bound to a pentamer. In this case, we indeed observed a more homogeneous but still high protein surface coverage on the l_o phase. Taking full protein coverage into account would theoretically lead to about 6–10 Gb_3-C24:1 molecules and about 3–5 Gb_3-C24:1-2OH molecules bound per pentamer (ESI†), which is still a sufficiently large number to strongly bind the protein onto the membrane taking into account that the high affinity binding sites of the protein are occupied first.[51] Of note, there are indications that Gb_3 might be buried as a result of glycosphingolipid specific interactions with cholesterol, an aspect that we cannot exclude as all membranes contained cholesterol.[12,53,54]

Our rough calculations suggest that the number of recruited Gb_3 molecules to the STxB pentamer is greatly influenced by the fatty acid of the Gb_3 molecule. This difference in lipid recruitment also influences the membrane organization more globally. In case of membranes containing Gb_3 with an α-hydroxylated fatty acid, a significant protein-induced lipid resorting is observed resulting in a significantly increased l_o phase area fraction (21% for Gb_3-C24:0-2OH, 17% for Gb_3-C24:1-2OH). However, neither for Gb_3-C24:1 nor for Gb_3-C24:0 containing membranes a substantial increase in l_o phase area fraction was observed.

From our results we conclude that the unsaturated Gb_3 species are the most important ones for the first step of Shiga

toxin internalization. Even though they have a much larger area demand than the saturated species, they still get clustered underneath the protein. This in turn would lead to an asymmetric reduction in membrane area, which is proposed to be prerequisite for membrane invaginations. This idea can be supported by the observation that in case of Gb_3-C24:1 the l_o phase gets reorganized and further phase-separated leading to a STxB decorated phase that contains more unsaturated lipid species, which would imply a lower bending modulus.[55] Reorganization of l_o phase lipid components have also been described by Safouane *et al.*, who found a protein-induced cosorting of l_o phase lipids into membrane tubes.[40] In contrast, the saturated species form very compact protein clusters, which recruit most of the Gb_3 molecules. However, these structures might be too rigid to allow for an energetically favourable bending of the membrane. The hydroxylated Gb_3 species foster large membrane reorganization, which might be of importance in the following processes once Shiga toxin has generated invaginations such as scission of the membrane[6] and lipid sorting upon transport along the retrograde route.

Conclusions

Prerequisite for understanding the impact of individual Gb_3 species on the phase behaviour of lipid membranes and their ability to bind STxB is a chemical access to pure Gb_3s. We developed a modular chemical approach that can be adapted to other glycosphingolipids, starting with three monosaccharide building blocks, sphingosine and different fatty acids. Chemical synthesis resulted in four Gb_3 species, which constitute the major fraction of Gb_3 in different cell types in nature. Reconstituted into phase-separated lipid membranes, these different Gb_3 molecules turned out to significantly influence the overall membrane organization even though the bilayers contained only 5 mol% of the globoside.

Protein cluster formation and lipid redistribution are discussed to be of major importance in the first step of the internalization process of Shiga toxin and Shiga-like toxins giving rise to the infection of cells. From our results we conclude that the unsaturated Gb_3 species are the most important ones for the first step of Shiga toxin internalization as binding of STxB leads to protein clusters concomitant with a large area demand of the lipids and probably a lower bending modulus owing to the unsaturation compared to saturated ones. This would lead to an asymmetric reduction in membrane area, which is proposed to be prerequisite for membrane invaginations induced by Shiga toxin.

Acknowledgements

Financial support by the DFG (SFB 803) is greatly acknowledged. D.B.W. is grateful to the DFG (Emmy Noether and Heisenberg Fellowships) and to the Fonds der Chemischen Industrie (Dozentenstipendium). W.R. acknowledges the support by the Excellence Initiative of the German Research Foundation (EXC 294), by the Ministry of Science, Research and the Arts of Baden-Württemberg (Az: 33-7532.20) and by the European Research Council (Programme "Ideas" – call identifier: ERC-2011-StG 282105). O.M.S. thanks the GGNB (PBCS) for a Ph.D. fellowship, A.R. thanks the Konrad-Adenauer Foundation for a Ph.D. fellowship. The authors thank Jutta Gerber-Nolte for technical assistance.

References

1 H. Ewers, W. Römer, A. E. Smith, K. Bacia, S. Dmitrieff, W. Chai, R. Mancini, J. Kartenbeck, V. Chambon, L. Berland, A. Oppenheim, G. Schwarzmann, T. Feizi, P. Schwille, P. Sens, A. Helenius and L. Johannes, *Nat. Cell Biol.*, 2010, **12**, 11–18.
2 B. Tsai, J. M. Gilbert, T. Stehle, W. Lencer, T. L. Benjamin and T. A. Rapoport, *EMBO J.*, 2003, **22**, 4346–4355.
3 T. Waddell, A. Cohen and C. A. Lingwood, *Proc. Natl. Acad. Sci. U. S. A.*, 1990, **87**, 7898–7901.
4 M. S. Jacewicz, M. Mobassaleh, S. K. Gross, K. A. Balasubramanian, P. F. Daniel, S. Raghavan, R. H. McCluer and G. T. Keusch, *J. Infect. Dis.*, 1994, **169**, 538–546.
5 F. Mallard, C. Antony, D. Tenza, J. Salamero, B. Goud and L. Johannes, *J. Cell Biol.*, 1998, **143**, 973–990.
6 W. Römer, L. Berland, V. Chambon, K. Gaus, B. Windschiegl, D. Tenza, M. R. E. Aly, V. Fraisier, J.-C. Florent, D. Perrais, C. Lamaze, G. Raposo, C. Steinem, P. Sens, P. Bassereau and L. Johannes, *Nature*, 2007, **450**, 670–675.
7 O. Kovbasnjuk, M. Edidin and M. Donowitz, *J. Cell Sci.*, 2001, **114**, 4025–4031.
8 T. Hanashima, M. Miyake, K. Yahiro, Y. Iwamaru, A. Ando, N. Morinaga and M. Noda, *Microb. Pathog.*, 2008, **45**, 124–133.
9 B. Windschiegl, A. Orth, W. Römer, L. Berland, B. Stechmann, P. Bassereau, L. Johannes and C. Steinem, *PLoS One*, 2009, **4**, e6238.
10 A. Orth, L. Johannes, W. Römer and C. Steinem, *ChemPhysChem*, 2012, **13**, 108–114.
11 L. Johannes and S. Mayor, *Cell*, 2010, **142**, 507–510.
12 C. A. Lingwood, *Cold Spring Harbor Perspect. Biol.*, 2011, **3**, a004788.
13 B. Binnington, D. Lingwood, A. Nutikka and C. A. Lingwood, *Neurochem. Res.*, 2002, **27**, 807–813.
14 W. Römer, L.-L. Pontani, B. Sorre, C. Rentero, L. Berland, V. Chambon, C. Lamaze, P. Bassereau, C. Sykes, K. Gaus and L. Johannes, *Cell*, 2010, **140**, 540–553.
15 A. Kiarash, B. Boyd and C. A. Lingwood, *J. Biol. Chem.*, 1994, **269**, 11138–11146.
16 O. Ekholm, S. Jaikishan, M. Lönnfors, T. K. Nyholm and J. P. Slotte, *Biochim. Biophys. Acta*, 2011, **1808**, 727–732.
17 J. Prades, S. S. Funari, M. Gomez-Florit, O. Vögler and F. Barceló, *Mol. Membr. Biol.*, 2012, **29**, 333–343.
18 B. Windschiegl and C. Steinem, *Langmuir*, 2006, **22**, 7454–7457.
19 A. Pellizzari, H. Pang and C. A. Lingwood, *Biochemistry*, 1992, **31**, 1363–1370.
20 A. J. García-Sáez, S. Chiantia and P. Schwille, *J. Biol. Chem.*, 2007, **282**, 33537–33544.

21 A. J. García-Sáez and P. Schwille, *FEBS Lett.*, 2010, **584**, 1653–1658.
22 S. Faiss, S. Schuy, D. Weiskopf, C. Steinem and A. Janshoff, *J. Phys. Chem. B*, 2007, **111**, 13979–13986.
23 S. L. Veatch and S. L. Keller, *Biochim. Biophys. Acta*, 2005, **1746**, 172–185.
24 D. C. Smith, D. J. Sillence, T. Falguières, R. M. Jarvis, L. Johannes, J. M. Lord, F. M. Platt and L. M. Roberts, *Mol. Biol. Cell*, 2006, **17**, 1375–1387.
25 H. Raa, S. Grimmer, D. Schwudke, J. Bergan, S. Wälchli, T. Skotland, A. Shevchenko and K. Sandvig, *Traffic*, 2009, **10**, 868–882.
26 S. J. Danishefsky and S. J. Keding, *US Pat.*, 0 208 884, 2004.
27 (*a*) A. Düfert and D. B. Werz, *J. Org. Chem.*, 2008, **73**, 5514–5519; (*b*) O. J. Plante, R. B. Andrade and P. H. Seeberger, *Org. Lett.*, 1999, **1**, 211–214.
28 I. J. Kim, T. K. Park, S. Hu, K. Abrampah, S. Zhang, P. Livingston and S. J. Danishefsky, *J. Org. Chem.*, 1995, **60**, 7716–7717.
29 (*a*) D. B. Werz, B. Castagner and P. H. Seeberger, *J. Am. Chem. Soc.*, 2007, **129**, 2770–2771; (*b*) O. J. Plante, E. R. Palmacci, R. B. Andrade and P. H. Seeberger, *J. Am. Chem. Soc.*, 2001, **123**, 9545–9554.
30 A. V. Demchenko, E. Rousson and G.-J. Boons, *Tetrahedron Lett.*, 1999, **40**, 6523–6526.
31 X. Zhu and R. R. Schmidt, *Angew. Chem., Int. Ed.*, 2009, **48**, 1900–1934.
32 Y. Iwayama, H. Ando, H. Ishida and M. Kiso, *Chem.–Eur. J.*, 2009, **15**, 4637–4648.
33 (*a*) D. A. Konen, L. S. Silbert and P. E. Pfeffer, *J. Org. Chem.*, 1975, **40**, 3253–3258; (*b*) J. E. Patterson, I. R. Ollmann, B. F. Cravatt, D. L. Boger, C.-H. Wong and R. A. Lerner, *J. Am. Chem. Soc.*, 1996, **118**, 5938–5945.
34 P. Zimmermann and R. R. Schmidt, *Liebigs Ann. Chem.*, 1988, **1988**, 663–667.
35 L. A. Carpino, A. El-Faham and F. Albericio, *J. Org. Chem.*, 1995, **60**, 3561–3564.
36 D. M. C. Ramirez, W. W. Ogilvie and L. J. Johnston, *Biochim. Biophys. Acta*, 2010, **1798**, 558–568.
37 S. Veatch and S. Keller, *Phys. Rev. Lett.*, 2005, **94**, 148101.
38 T. Baumgart, G. Hunt, E. R. Farkas, W. W. Webb and G. W. Feigenson, *Biochim. Biophys. Acta*, 2007, **1768**, 2182–2194.
39 R. M. A. Sullan, J. K. Li, C. Hao, G. C. Walker and S. Zou, *Biophys. J.*, 2010, **99**, 507–516.
40 M. Safouane, L. Berland, A. Callan-Jones, B. Sorre, W. Römer, L. Johannes, G. E. S. Toombes and P. Bassereau, *Traffic*, 2010, **11**, 1519–1529.
41 H. Ling, A. Boodhoo, B. Hazes, M. D. Cummings, G. D. Armstrong, J. L. Brunton and R. J. Read, *Biochemistry*, 1998, **37**, 1777–1788.
42 N. Bezlyepkina, R. S. Gracià, P. Shchelokovskyy, R. Lipowsky and R. Dimova, *Biophys. J.*, 2013, **104**, 1456–1464.
43 C. S. Scheve, P. A. Gonzales, N. Momin and J. C. Stachowiak, *J. Am. Chem. Soc.*, 2013, **135**, 1185–1188.
44 A. J. Sodt, M. L. Sandar, K. Gawrisch, R. W. Pastor and E. Lyman, *J. Am. Chem. Soc.*, 2014, **136**, 725–732.
45 B. Ramstedt, P. Leppimäki, M. Axberg and J. P. Slotte, *Eur. J. Biochem.*, 1999, **266**, 997–1002.
46 H. Löfgren and I. Pascher, *Chem. Phys. Lipids*, 1977, **20**, 273–284.
47 C. Yuan and L. J. Johnston, *Biophys. J.*, 2001, **81**, 1059–1069.
48 D. Marsh, *Biochim. Biophys. Acta*, 2009, **1788**, 2114–2123.
49 G. W. Feigenson, *Biochim. Biophys. Acta*, 2009, **1788**, 47–52.
50 A. E. Garner, D. A. Smith and N. M. Hooper, *Mol. Membr. Biol.*, 2007, **24**, 233–242.
51 D. Pina, L. Johannes and M. Castanho, *Biochim. Biophys. Acta*, 2007, **1768**, 628–636.
52 J. Shi, T. Yang, S. Kataoka, Y. Zhang, A. J. Diaz and P. S. Cremer, *J. Am. Chem. Soc.*, 2007, **129**, 5954–5961.
53 D. Lingwood, B. Binnington, T. Róg, I. Vattulainen, M. Grzybek, Ü. Coskun, C. A. Lingwood and K. Simons, *Nat. Chem. Biol.*, 2011, **7**, 260–262.
54 R. Mahfoud, A. Manis, B. Binnington, C. Ackerley and C. A. Lingwood, *J. Biol. Chem.*, 2010, **285**, 36049–36059.
55 T. Baumgart, S. T. Hess and W. W. Webb, *Nature*, 2003, **425**, 821–824.